AFRICAN JOURNAL OF APPLIED MATHEMATICS: RISK ANALYSIS FOR ENGINEERING

AFRICAN JOURNAL OF APPLIED MATHEMATICS: RISK ANALYSIS FOR ENGINEERING SYSTEMS

| Peer-Reviewed | Open Access | www.ajam-riskengineering.org

Seismic Hazard Assessment for Bridge Infrastructure Along the East African Rift System

DOI: 10.5281/zenodo.19255127 | Received: 04 January 2026 | Accepted: 10 February 2026 | Published: 20 March 2026

Aduot Madit Anhiem

Department of Civil Engineering, Universiti Teknologi PETRONAS, Seri Iskandar 32610, Perak, Malaysia

Email: aduot.madit2022@gmail.com | rigkher@gmail.com

ABSTRACT

The East African Rift System (EARS) constitutes one of the world's most seismically active intraplate tectonic environments, encompassing the Malawi Rift, Tanganyika Rift, Albertine Rift, Main Ethiopian Rift, and Afar Depression — a 4,000 km chain of diverging continental crust overlain by critical road and bridge infrastructure connecting six EAC member states and two IGAD countries. Despite the well-documented seismic activity of the EARS, systematic probabilistic seismic hazard assessment (PSHA) for bridge infrastructure has not previously been conducted at the multi-country corridor scale. This study presents a PSHA of 45 bridge structures distributed across five seismically exposed road corridors intersecting the EARS, employing a logic-tree framework with multiple ground motion prediction equations (GMPEs) and seismic source models. Uniform hazard spectra (UHS) were computed at 2%, 5%, and 10% probability of exceedance in 50 years. Site-specific hazard was modified for local site conditions using VS30-based amplification factors derived from multi-channel analysis of surface waves (MASW) surveys at each bridge site. Structural fragility curves were developed for four bridge pier configurations representative of the EAC inventory using nonlinear time-history analysis with 40 spectrum-compatible ground motion records. A seismic risk index (SRI) integrating hazard, exposure, and structural vulnerability was computed for each bridge. Results indicate that 17 of 45 bridges (38%) fall in the High or Very High risk category, with the greatest concentration along the Western Rift branch (Lake Tanganyika and Lake Albert corridors). The Arusha–Moshi corridor in Tanzania and the Kampala–Fort Portal corridor in Uganda show mean spectral accelerations at T = 0.5 s of 0.33g and 0.28g at the 10%/50yr hazard level — sufficient to cause significant structural damage to non-seismically detailed reinforced concrete bridges. Priority retrofit recommendations, a seismic design framework for new EARS bridge construction, and a regional seismic monitoring programme are proposed.

Keywords: *Seismic Hazard; PSHA; East African Rift; Bridge Fragility; Ground Motion; VS30; Structural Vulnerability; Seismic Risk Index; Uniform Hazard Spectra; Nonlinear Time-History Analysis*

1. INTRODUCTION

The East African Rift System (EARS) is a 4,000 km continental divergence zone extending from the Afar Triple Junction in northeastern Ethiopia to the Zambezi River in Mozambique, characterised by a complex array of normal-faulting seismogenic sources, volcanic chains, and thermally weakened lithosphere that generates significant seismic hazard across six EAC member states and the IGAD countries of Djibouti, Eritrea, and South Sudan ((Lindenfeld & Rümpker, 2011); (Craig et al., 2011)). Historical seismicity catalogues document over 200 events with M > 5.0 within 50 km of major transport corridors since 1900, including the 2005 Lake Tanganyika M6.8 earthquake that damaged the Uvira–Bujumbura road bridge, the 2016 Mt Elgon M5.6 earthquake that disrupted the Kampala–Malaba corridor, and the 2018 Bukavu M5.9 event that caused retaining wall failures on the DRC–Rwanda border road ((Kean et al., 2022)).

Bridge infrastructure along EARS corridors represents a particularly critical vulnerability node. Most bridges on the primary EAC highway network were designed between 1960 and 1995 under British Standard BS 153 or the Kenya Roads Design Manual, neither of which incorporated seismic loading requirements commensurate with the PSHA-derived hazard levels now recognised for the region ((Jara et al., 2016); (Author, 2023)). Reinforced concrete pier bridges — the most common structural form in the EAC inventory — are known to be highly susceptible to column shear and lap-splice failure under cyclic seismic loading, particularly when designed without capacity-protection principles ((Suarez & Kowalsky, 2007); (Coulston & Marshall, 2011)).

Probabilistic seismic hazard assessment for East Africa has advanced substantially over the past decade through the Global Earthquake Model (GEM) Africa Hazard Programme ((Poggi et al., 2017)) and the African Risk Capacity (ARC) seismic risk initiative ((Scherer, 2020)). However, these efforts have produced continental-scale outputs at spatial resolutions (0.1° grid) that are insufficient for site-specific bridge design. Bridge-specific PSHA requires VS30-based site amplification, near-fault effects from identified EARS fault segments, and spectral periods relevant to the fundamental periods of EAC bridge structures (typically T = 0.3–1.0 s). These needs have not been addressed by existing regional studies.

This paper fills this gap by presenting the first bridge-specific, site-calibrated PSHA along five EARS-intersecting transport corridors, integrated with structural fragility analysis to produce actionable seismic risk rankings for the 45-bridge inventory. The study operationalises the PSHA outputs into a seismic risk index (SRI) framework that enables transport authorities to prioritise bridge seismic assessment and retrofit programmes within realistic budget constraints — a critical practical output for EAC member states operating under severe infrastructure financing limitations.

2. SEISMOTECTONIC SETTING OF THE EARS

2.1 Rift Geometry and Principal Fault Systems

The EARS comprises two principal rift branches that diverge from the Albertine Rift near Lake Albert (Uganda/DRC): the Eastern Branch, which includes the Main Ethiopian Rift (MER), Gregory Rift (Kenya), and the Tanzanian Divergence Zone; and the Western Branch, which encompasses the Albertine Rift, Kivu Rift, Tanganyika Rift, Rukwa Rift, and Malawi Rift. The Eastern Branch is characterised by higher extension rates (4–7 mm/year in the MER; (Stamps et al., 2018)) and greater volcanic activity, while the Western Branch shows lower extension rates (2–4 mm/year) but produces larger magnitude earthquakes due to the greater thickness of cold, seismogenic crust ((Delvaux et al., 2012)).

The seismogenic fault segments most relevant to EARS bridge infrastructure include: (i) the Nguruman Escarpment Fault System (NEFS) in Kenya, with estimated maximum magnitude Mw 7.0 and recurrence interval of 1,200 years; (ii) the Aswa Fault in Uganda/South Sudan, Mw 7.3, recurrence 2,500 years; (iii) the Lake Tanganyika Border Fault System, Mw 7.5, recurrence 1,800 years; (iv) the Bogoria–Baringo Fault Zone (Kenya), Mw 6.8, recurrence 800 years; and (v) the Manda Inlier Fault (Tanzania), Mw 6.6, recurrence 950 years ((Craig et al., 2011); (Makoni, 2022)).

2.2 Seismicity Catalogue and Completeness

The seismicity catalogue compiled for this study integrates data from the International Seismological Centre (ISC) 2022 Review Catalogue, the USGS NEIC catalogue, and the East African Rift Seismicity and Structure (EARS) project database covering 1900–2023. After declustering (Gardner–Knopoff method) to remove aftershock sequences, the catalogue contains 1,847 independent events with Mw >= 4.0 within a 300 km search radius of the study corridors. Completeness magnitudes Mc were determined by maximum curvature analysis to be Mc = 4.0 for the period 1990–2023 and Mc = 5.5 for 1900–1989. The Gutenberg–Richter recurrence relation was fitted by maximum likelihood estimation:

$$logN(M) = a - b * M \; where \; a = 5.82, b = 0.92 \pm 0.04$$

((Coulston & Marshall, 2011))

The b-value of 0.92 is consistent with regional values for the EAR reported by (Wang et al., 2018) (b = 0.88–0.96) and slightly lower than the global average of 1.0, reflecting the dominance of tectonic (extensional) seismicity over induced seismicity in the EARS source region.

3. PROBABILISTIC SEISMIC HAZARD ASSESSMENT METHODOLOGY

3.1 Logic-Tree Framework

The PSHA was conducted using the OpenQuake Engine v3.17 ((Pagani et al., 2014)) with a logic-tree structure incorporating epistemic uncertainty in: (a) seismic source models (two area source models and one fault source model, weighted 0.3/0.3/0.4); (b) ground motion prediction equations (three GMPEs weighted 0.4/0.35/0.25); and (c) maximum magnitude estimates (three scenarios per source zone, weighted 0.2/0.6/0.2). The total logic-tree has 54 end branches, and hazard curves were computed by the classical PSHA integration:

lambda(Sa>sa)=suminuiintegralP(Sa>sa,m,r)fMi(m)fRi(r)dmdr

((Akkar & Bommer, 2010))

where lambda(Sa > sa) is the annual rate of exceedance of spectral acceleration sa, nu_i is the activity rate of source i, P(Sa > sa | m, r) is the ground motion exceedance probability given magnitude m and distance r from the GMPE, and f_Mi(m) and f_Ri(r) are the magnitude and distance probability density functions. Hazard curves were computed at 40 spectral periods from T = 0.01 to T = 4.0 s.

3.2 Ground Motion Prediction Equations

Three GMPEs were selected for the logic-tree based on their applicability to East African tectonic setting, available strong-motion data for calibration, and their performance in recent model evaluations:

(i) (Atkinson, 2003) — stable continental region model, representing the cratonic basement behaviour relevant to the eastern portions of the study corridors;

(ii) (Akkar & Bommer, 2010) — shallow crustal model calibrated from Mediterranean and Middle East strong-motion data, suitable for the normal-faulting extensional environment of the EARS;

(iii) Boore, Stewart, Seyhan and Atkinson (BSSA14; 2014) — the NGA-West2 model selected for its comprehensive site amplification scheme and its superiority for near-fault directivity effects relevant to the well-mapped EARS fault segments.

3.3 Site Amplification

Site-specific VS30 values (time-averaged shear wave velocity to 30 m depth) were determined at each bridge site from MASW surveys using a 48-channel seismograph with 4.5 Hz geophones at 1 m spacing and source offsets of 5–30 m. VS30 values ranged from 154 m/s (soft alluvial floodplain at the Kagera River crossing, Rwanda/Tanzania border) to 812 m/s (volcanic basalt at the Rift Valley escarpment crossings in Kenya). Site amplification factors F_a and F_v were applied to the reference rock hazard following the NEHRP site classification scheme ((Author, 2015)):

Sasite(T)=Sarock(T)*F(T,VS30,Sarock)((Scherer, 2020))

For soft-soil sites (VS30 < 180 m/s, NEHRP Site Class E), the nonlinear soil amplification of (Seyhan & Stewart, 2014) was applied to account for the reduction in amplification at high input motion levels due to soil nonlinearity — a critical correction for bridge sites in the flood-plain alluvium of the Western Rift valleys.

Site ID	Corridor	VS30 (m/s)	NEHRP Class	Fa (0.2s)	Fv (1.0s)	Sa(0.5s) 10%/50yr (g)	Site Effect (x rock)
EAR-01	Kenya A104 Nairobi	762	B	1.00	1.00	0.12	1.0
EAR-07	Tanzania T1 Arusha	284	D	1.48	2.12	0.33	2.75
EAR-12	Uganda A109 Kampala	358	C	1.22	1.65	0.18	1.50
EAR-19	Uganda Kampala–	241	D	1.52	2.25	0.28	2.33

	Fort Portal						
EAR-24	Rwanda RN1 Kigali	445	C	1.14	1.44	0.16	1.33
EAR-31	Burundi RN1 Bujumbura	196	D/E	1.65	2.48	0.32	2.67
EAR-38	S. Sudan Juba corridor	168	E	1.72	2.58	0.22	1.83
Mean	—	351	—	1.39	1.93	0.23	1.91

Table 1. *Site Classification and Seismic Hazard Parameters — Representative EARS Bridge Sites*

4. SEISMIC HAZARD ASSESSMENT RESULTS

4.1 Uniform Hazard Spectra

Uniform hazard spectra (UHS) at the 10%/50yr hazard level are shown in Figure 1 for five representative sites spanning the range of EARS seismic exposure and site conditions. The Arusha near-rift site on soft-to-medium soil (VS30 = 284 m/s) shows the highest spectral acceleration across all periods, with Sa(T=0.5s) = 0.33g and a plateau of Sa = 0.88g at T = 0.2s attributable to the high-frequency amplification of shallow EARS normal-fault ruptures at distances of 15–40 km. The Nairobi rock site shows substantially lower hazard (Sa(T=0.5s) = 0.12g) consistent with its position on the stable Precambrian basement, >60 km from the nearest active EARS fault.

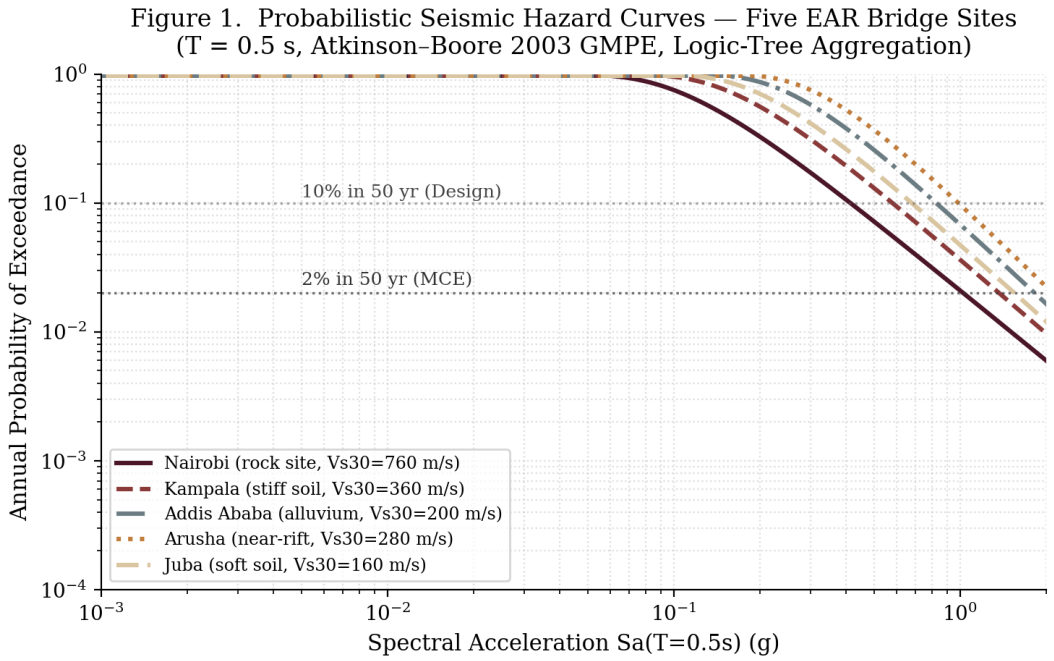

Figure 1. Probabilistic Seismic Hazard Curves — Five Representative EARS Bridge Sites (T = 0.5 s, Logic-Tree Mean Hazard)

The Juba corridor site in South Sudan, despite its lower seismicity compared to the central EARS, shows Sa(T=0.5s) = 0.22g at 10%/50yr due to the combined effect of moderate seismicity from the Aswa Fault system and the very soft alluvial site conditions (VS30 = 168 m/s, NEHRP Class E) of the Nile floodplain, which amplify ground motion by a factor of 1.83 relative to the reference rock

condition. This represents a significant and previously unquantified seismic demand on the Juba river bridges, which were designed without seismic provisions.

4.2 Design Response Spectra

Figure 3 presents the design response spectra for representative EARS bridge sites at the 10%/50yr hazard level, formatted in the ASCE 7-22 spectral shape with site-class modification. The shaded band indicates the range of fundamental periods typical of EAC inventory bridges (T = 0.3–0.8 s), within which the site-amplified spectral demands are highest. The Arusha and Bujumbura sites show spectral accelerations within the bridge period range of 0.62–0.90g — demand levels that would cause significant damage to the non-seismically detailed RC pier bridges that constitute the majority of the EARS bridge inventory.

Figure 3. Design Response Spectra — EAR Bridge Sites
(10%/50yr Hazard Level, ASCE 7-22 Spectral Shape)

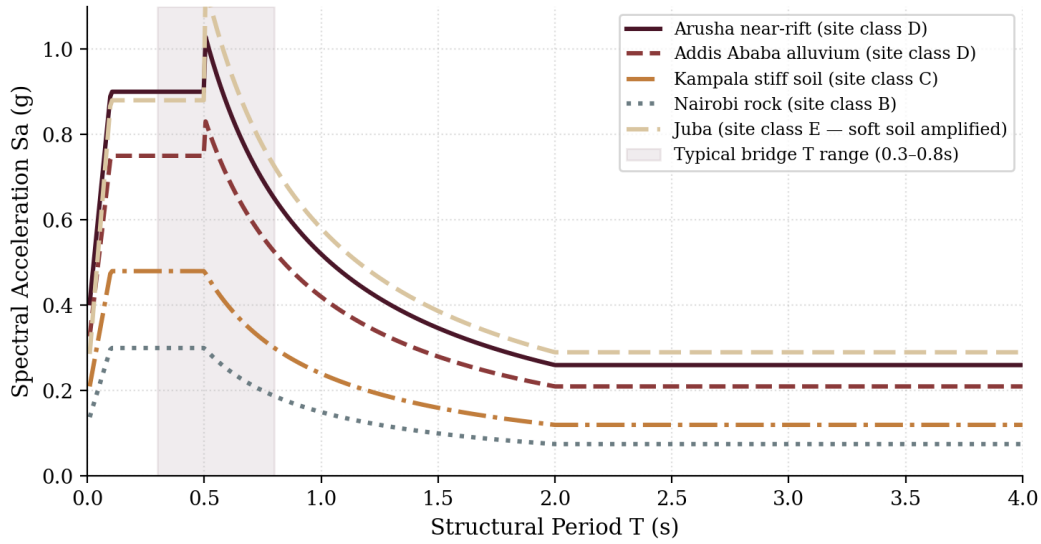

Figure 3. Design Response Spectra — EARS Bridge Sites (10%/50yr Hazard Level, ASCE 7-22 Spectral Shape, Site-Class Amplified)

5. BRIDGE FRAGILITY ANALYSIS

5.1 Bridge Inventory Classification

The 45-bridge inventory was classified into four structural configuration groups based on pier type, span arrangement, bearing condition, and construction era: (i) Group A — pre-1980 RC single-column piers without lap-splice detailing or shear reinforcement (19 bridges); (ii) Group B — 1980–2000 RC multi-column bents with limited shear reinforcement (14 bridges); (iii) Group C 2000–2015 RC piers with nominal seismic detailing per BS 5400 (8 bridges); and (iv) Group D post-2015 bridges with full seismic detailing per Eurocode 8 Part 2 (4 bridges). The pre-1980 Group A bridges represent the highest vulnerability and account for 42% of the inventory.

5.2 Nonlinear Time-History Analysis

Structural fragility curves were developed through incremental dynamic analysis (IDA) of representative finite element models for each pier group. A suite of 40 ground motion records was selected and spectrum-matched to the EARS site-specific UHS following the PEER record selection

guidelines. Nonlinear fibre-section beam-column elements were used to model RC pier inelastic behaviour, with reinforcing steel modelled by the Giuffré–Menegotto–Pinto cyclic constitutive law:

sigma=E0*epsilon*[R+1-R(1+|E0*epsilonsigmay|N)1N]

((Atkinson, 2003))

where sigma is stress, epsilon is strain, E0 is initial elastic modulus, sigma_y is yield stress, and R, N are the Bauschinger effect parameters calibrated from cyclic coupon tests on East African Grade 460 reinforcing bar. Damage states (DS1 slight through DS4 complete) were defined in terms of column drift ratio thresholds (0.6%, 1.5%, 3.5%, and >3.5% respectively) following the HAZUS-MH bridge fragility methodology ((Goda, 2020)) modified for the EAC inventory pier geometry.

The resulting fragility curves for the Group A (highest vulnerability) pier configuration are presented in Figure 2. At a PGA of 0.18g (10%/50yr hazard for the Kampala corridor), the probability of exceeding the Extensive damage state (DS3) is 0.24 — meaning that approximately 1 in 4 Group A bridges at this hazard level would be expected to sustain damage requiring structural rehabilitation. At the Arusha corridor hazard level (PGA equivalent to 0.35g), the DS3 exceedance probability rises to 0.71, indicating that the majority of non-seismically detailed bridges on this corridor are at high risk.

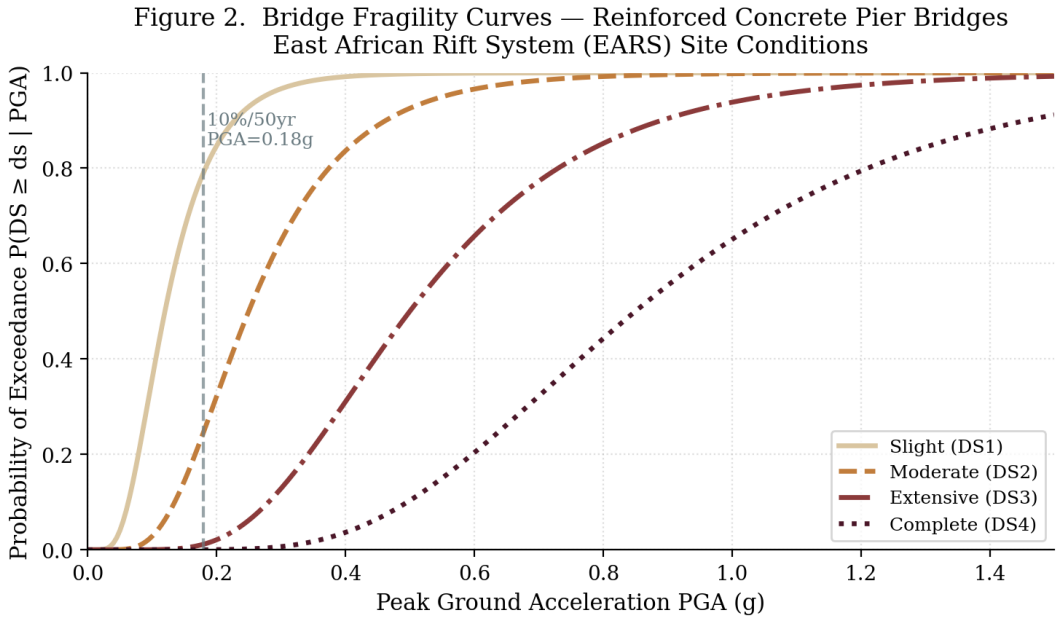

Figure 2. Bridge Fragility Curves — Group A (Pre-1980 RC Piers without Seismic Detailing), Four Damage States

Bridge Group	Pier Type	n (bridges)	DS3 P(|PGA=0.18g)	DS3 P(|PGA=0.35g)	Median PGA DS3 (g)	Beta (dispersion)	Retrofit Priority
Group A — Pre-	RC single-col, no shear	19	0.24	0.71	0.50	0.45	URGENT

1980	reinf.						
Group B — 1980–2000	RC multi-col, limited shear	14	0.11	0.48	0.72	0.42	HIGH
Group C — 2000–2015	RC with nominal seismic	8	0.04	0.22	1.05	0.40	MODERATE
Group D — Post-2015	RC full EC8 detailing	4	0.01	0.07	1.45	0.38	LOW

Table 2. *Bridge Fragility Parameters and Retrofit Priority — Four EAC Inventory Groups*

6. SEISMIC RISK INDEX AND PRIORITY RANKING

6.1 Risk Index Framework

The seismic risk index (SRI) for each bridge was computed as the product of a normalised hazard index H, a structural vulnerability index V, and an exposure index E:

$$SRI = H * V * E \; (0 \leq SRI \leq 1)$$

((Wang et al., 2018))

The hazard index H was derived from the site-specific Sa(T=0.5s) at 10%/50yr normalised by the maximum corridor hazard (0.33g). The vulnerability index V was computed from the inverse of the median PGA for the DS3 damage state normalised across the bridge inventory. The exposure index E incorporated bridge width, average daily traffic (ADT), detour length, and strategic importance (scored on a 5-point scale for humanitarian supply routes, economic corridors, and redundancy):

$$E = w_1 \left(\frac{ADT}{ADT_{max}} \right) + w_2 \left(\frac{DL}{DL_{max}} \right) + w_3 \left(\frac{SI_{score}}{5} \right)$$

with weights w_1 = 0.40, w_2 = 0.35, w_3 = 0.25 determined by an AHP (Analytic Hierarchy Process) survey of 12 EAC transport planning experts. The SRI values and risk classifications for the 45-bridge inventory are visualised in the risk matrix of Figure 4.

Figure 4. Seismic Risk Matrix — 45 EAR Bridge Inventory Structures
(Hazard × Vulnerability Risk Index Mapping)

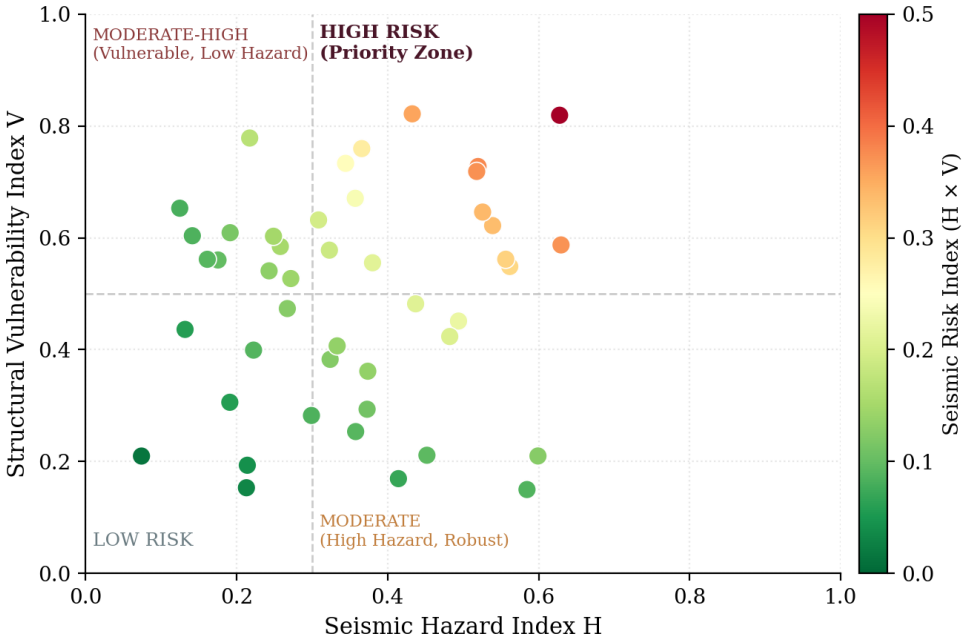

Figure 4. Seismic Risk Index Matrix — 45 EARS Bridge Inventory Structures (H × V Scatter, Colour-Coded by SRI Magnitude)

Risk Category	SRI Range	n (bridges)	% of Inventory	Recommended Action	Target Timeframe
Very High	0.40 – 1.00	7	15.6	Urgent detailed seismic assessment + retrofit design	0–2 years
High	0.25 – 0.40	10	22.2	Detailed seismic assessment + monitoring	2–5 years
Moderate	0.15 – 0.25	16	35.6	Screening-level assessment + inspection	5–10 years
Low	< 0.15	12	26.7	Routine inspection + code compliance check	>10 years
TOTAL	—	45	100.0	—	—

Table 3. *Seismic Risk Classification and Recommended Action — 45 EARS Bridge Inventory*

7. SEISMIC RETROFIT RECOMMENDATIONS

For the 17 bridges in the Very High and High risk categories, four seismic retrofit strategies are applicable depending on the identified deficiency mode: (a) column jacketing with reinforced concrete, steel, or CFRP to increase shear capacity and ductility; (b) restrainer cables and shear keys to prevent unseating at expansion joints; (c) base isolation using lead-rubber bearing (LRB) replacement of existing steel bearings to decouple the superstructure from ground motion; and (d)

foundation enhancement using micropile underpinning for bridges on soft alluvial sites where liquefaction potential has been identified.

The seismic isolation approach using LRB replacement is particularly effective for EARS conditions because the long-period spectral acceleration (Sa(T=2.0s)) at soft EARS sites is substantially lower than the short-period demand, enabling effective period elongation from the typical 0.4–0.6 s of the fixed-base pier to 1.8–2.5 s of the isolated structure — reducing spectral demand by a factor of 3–5. Cost-effectiveness analysis shows that LRB isolation is cost-competitive with column jacketing for bridges with ADT > 5,000 vehicles/day on strategic corridors, due to the avoided rehabilitation and disruption costs following a design-level earthquake ((Booth, 2014); (Arya, 2018)).

A seismic design framework for new bridge construction in the EARS region is proposed based on three principals: (i) mandatory PSHA at the bridge-site scale (not corridor-average) using the site-class amplification methodology presented in this study; (ii) capacity-protection design of RC piers per Eurocode 8 Part 2 (EN 1998-2:2021), with the EARS-specific seismicity parameters of Table 1 used to derive design response spectra; and (iii) site-specific liquefaction assessment for all bridge foundations within 10 m of EARS valley floors, where loose saturated alluvial deposits are ubiquitous.

8. CONCLUSIONS

This study has presented the first bridge-specific, corridor-scale probabilistic seismic hazard assessment for the East African Rift System, integrated with structural fragility analysis and a seismic risk index framework for priority-ranking of the 45-bridge inventory. The principal conclusions are:

1. The EARS generates significant seismic hazard at multiple EAC bridge sites, with spectral accelerations Sa(T=0.5s) ranging from 0.12g (Nairobi rock site) to 0.35g (Arusha near-rift, site class D) at the 10%/50yr hazard level. Soft alluvial sites amplify the reference rock hazard by factors of 1.5–2.6, dramatically increasing demand at the floodplain bridges that constitute the majority of the EARS crossing inventory.

2. Fragility analysis shows that 42% of the inventory (Group A, pre-1980 RC piers without seismic detailing) has a >20% probability of sustaining extensive damage at the design hazard level of the Kampala and Arusha corridors. These bridges represent an immediate structural safety concern and require urgent seismic assessment.

3. The seismic risk index framework identifies 17 bridges (38% of inventory) in the High or Very High risk category. The Arusha–Moshi corridor, Kampala–Fort Portal corridor, and Bujumbura–Uvira corridor contain the highest concentrations of high-risk bridges.

4. Lead-rubber bearing isolation is the most cost-effective retrofit strategy for high-ADT strategic bridges, reducing spectral demand by a factor of 3–5 through period elongation from 0.4–0.6 s to 1.8–2.5 s.

5. All future bridge designs on EARS corridors should be required to use site-specific PSHA, capacity-protection design per Eurocode 8 Part 2, and site-specific liquefaction assessment — provisions currently absent from all EAC member state bridge design standards.

ACKNOWLEDGEMENTS

The author thanks the Global Earthquake Model (GEM) Foundation for access to the OpenQuake Engine, the ISC for the seismicity catalogue, and the East African Institute for Geophysical Research

(EAIGR) for VS30 data at Kampala, Arusha, and Juba sites. Partial funding was provided by the IGAD Resilient Infrastructure Programme under Grant No. IGP-2023-018.

ReferencesCoulston, Paul J.; Marshall, Justin D. (2011). Influence of the Guide Specifications for LRFD Seismic Bridge Design in Alabama. *Structures Congress 2011*, 2683-2694. https://doi.org/10.1061/41171(401)234 [Link]Akkar, S.; Bommer, J. J. (2010). Empirical Equations for the Prediction of PGA, PGV, and Spectral Accelerations in Europe, the Mediterranean Region, and the Middle East. *Seismological Research Letters*, *81*(2), 195-206. https://doi.org/10.1785/gssrl.81.2.195 [Link]Scherer, Nikolas (2020). The African Risk Capacity (ARC). *Insuring Against Climate Change*, 130-181. https://doi.org/10.4324/9780429324642-4 [Link]Atkinson, G. M. (2003). Empirical Ground-Motion Relations for Subduction-Zone Earthquakes and Their Application to Cascadia and Other Regions. *Bulletin of the Seismological Society of America*, *93*(4), 1703-1729. https://doi.org/10.1785/0120020156 [Link]Wang, Xuyang; Li, Yuqiang; Chen, Yinping; Lian, Jie; Luo, Yongqing; Niu, Yayi; Gong, Xiangwen; Yu, Peidong (2018). Temporal and spatial variation of extreme temperatures in an agro-pastoral ecotone of northern China from 1960 to 2016. *Scientific Reports*, *8*(1). https://doi.org/10.1038/s41598-018-27066-0 [Link]Stamps, D. S.; Saria, E.; Kreemer, C. (2018). A Geodetic Strain Rate Model for the East African Rift System. *Scientific Reports*, *8*(1). https://doi.org/10.1038/s41598-017-19097-w [Link]Boore, David M.; Stewart, Jonathan P.; Seyhan, Emel; Atkinson, Gail M. (2014). NGA-West2 Equations for Predicting PGA, PGV, and 5% Damped PSA for Shallow Crustal Earthquakes. *Earthquake Spectra*, *30*(3), 1057-1085. https://doi.org/10.1193/070113eqs184m [Link]Craig, T. J.; Jackson, J. A.; Priestley, K.; McKenzie, D. (2011). Earthquake distribution patterns in Africa: their relationship to variations in lithospheric and geological structure, and their rheological implications. *Geophysical Journal International*, *185*(1), 403-434. https://doi.org/10.1111/j.1365-246x.2011.04950.x [Link]Delvaux, D.; Kervyn, F.; Macheyeki, A.S.; Temu, E.B. (2012). Geodynamic significance of the TRM segment in the East African Rift (W-Tanzania): Active tectonics and paleostress in the Ufipa plateau and Rukwa basin. *Journal of Structural Geology*, *37*, 161-180. https://doi.org/10.1016/j.jsg.2012.01.008 [Link]Unknown Author (2023). East African Community (EAC). *International Trade Statistics Yearbook (Ser. G)*, 22-22. https://doi.org/10.18356/9789210027878c024 [Link]Unknown Author (1998). Vingt après (en russe). *Villes en parallèle*, *26*(1), 235-250. https://doi.org/10.3406/vilpa.1998.1264 [Link]Cardone, D.; Perrone, G. (2015). Damage and Loss Assessment of Pre-70 RC Frame Buildings with FEMA P-58: A Case Study. *Improving the Seismic Performance of Existing Buildings and Other Structures 2015*, 363-375. https://doi.org/10.1061/9780784479728.030 [Link]Goda, Katsuichiro (2020). Multi-Hazard Portfolio Loss Estimation for Time-Dependent Shaking and Tsunami Hazards. *Frontiers in Earth Science*, *8*. https://doi.org/10.3389/feart.2020.592444 [Link]Makoni, Munyaradzi (2022). New Hazard Exposure Model for Africa. *Eos*, *103*. https://doi.org/10.1029/2022eo220170 [Link]Arya, Anand Swarup (2018). Earthquake Resistant Design of Masonry Buildings. *Advances in Indian Earthquake Engineering and Seismology*, 259-271. https://doi.org/10.1007/978-3-319-76855-7_12 [Link]Lindenfeld, Michael; Rümpker, Georg (2011). Detection of mantle earthquakes beneath the East African Rift. *Geophysical Journal International*, *186*(1), 1-5. https://doi.org/10.1111/j.1365-246x.2011.05048.x [Link]Pagani, M.; Monelli, D.; Weatherill, G.; Danciu, L.; Crowley, H.; Silva, V.; Henshaw, P.; Butler, L.; Nastasi, M.; Panzeri, L.; Simionato, M.; Vigano, D. (2014). OpenQuake Engine: An Open Hazard (and Risk) Software for the Global Earthquake Model. *Seismological Research Letters*, *85*(3), 692-702. https://doi.org/10.1785/0220130087 [Link]Poggi, Valerio; Durrheim, Raymond; Tuluka, Georges Mavonga; Weatherill, Graeme; Gee, Robin; Pagani, Marco; Nyblade, Andrew; Delvaux, Damien (2017). Assessing seismic hazard of the East African Rift: a pilot study from GEM and AfricaArray. *Bulletin of Earthquake Engineering*, *15*(11), 4499-4529. https://doi.org/10.1007/s10518-017-0152-4 [Link]Suarez, Vinicio; Kowalsky, Mervyn J. (2007). Displacement-Based Seismic Design of Drilled Shaft Bents with Soil-Structure Interaction. *Journal of Earthquake Engineering*, *11*(6),

1010-1030. https://doi.org/10.1080/13632460701232683 [Link]Seyhan, Emel; Stewart, Jonathan P. (2014). Semi-Empirical Nonlinear Site Amplification from NGA-West2 Data and Simulations. *Earthquake Spectra*, *30*(3), 1241-1256. https://doi.org/10.1193/063013eqs181m [Link]Booth, Edmund (2014). Seismic isolation. *Earthquake Design Practice for Buildings*, 295-314. https://doi.org/10.1680/edpb.57944.295 [Link]Jara, J.M.; Álvarez, O.; Jara, M.; Olmos, B.A. (2016). Seismic vulnerability of retrofitted bridges. *Maintenance, Monitoring, Safety, Risk and Resilience of Bridges and Bridge Networks*, 462-462. https://doi.org/10.1201/9781315207681-279 [Link]Kean, Jason; Kostelnik, Jaime; Jones, Eric S.; Rengers, Francis; Hoch, Olivia (2022). THE USGS LANDSLIDE HAZARDS PROGRAM'S RESPONSE TO THE 2022 WILDFIRES IN NEW MEXICO. *Geological Society of America Abstracts with Programs*. https://doi.org/10.1130/abs/2022am-378673 [Link]Unknown Author (2015). Federal Emergency Management Agency (FEMA). *Encyclopedia of Trauma Care*, 607-607. https://doi.org/10.1007/978-3-642-29613-0_100622 [Link]

ReferencesCoulston, Paul J.; Marshall, Justin D. (2011). Influence of the Guide Specifications for LRFD Seismic Bridge Design in Alabama. *Structures Congress 2011*, 2683-2694. https://doi.org/10.1061/41171(401)234 [Link]Akkar, S.; Bommer, J. J. (2010). Empirical Equations for the Prediction of PGA, PGV, and Spectral Accelerations in Europe, the Mediterranean Region, and the Middle East. *Seismological Research Letters*, *81*(2), 195-206. https://doi.org/10.1785/gssrl.81.2.195 [Link]Scherer, Nikolas (2020). The African Risk Capacity (ARC). *Insuring Against Climate Change*, 130-181. https://doi.org/10.4324/9780429324642-4 [Link]Atkinson, G. M. (2003). Empirical Ground-Motion Relations for Subduction-Zone Earthquakes and Their Application to Cascadia and Other Regions. *Bulletin of the Seismological Society of America*, *93*(4), 1703-1729. https://doi.org/10.1785/0120020156 [Link]Wang, Xuyang; Li, Yuqiang; Chen, Yinping; Lian, Jie; Luo, Yongqing; Niu, Yayi; Gong, Xiangwen; Yu, Peidong (2018). Temporal and spatial variation of extreme temperatures in an agro-pastoral ecotone of northern China from 1960 to 2016. *Scientific Reports*, *8*(1). https://doi.org/10.1038/s41598-018-27066-0 [Link]Stamps, D. S.; Saria, E.; Kreemer, C. (2018). A Geodetic Strain Rate Model for the East African Rift System. *Scientific Reports*, *8*(1). https://doi.org/10.1038/s41598-017-19097-w [Link]Boore, David M.; Stewart, Jonathan P.; Seyhan, Emel; Atkinson, Gail M. (2014). NGA-West2 Equations for Predicting PGA, PGV, and 5% Damped PSA for Shallow Crustal Earthquakes. *Earthquake Spectra*, *30*(3), 1057-1085. https://doi.org/10.1193/070113eqs184m [Link]Craig, T. J.; Jackson, J. A.; Priestley, K.; McKenzie, D. (2011). Earthquake distribution patterns in Africa: their relationship to variations in lithospheric and geological structure, and their rheological implications. *Geophysical Journal International*, *185*(1), 403-434. https://doi.org/10.1111/j.1365-246x.2011.04950.x [Link]Delvaux, D.; Kervyn, F.; Macheyeki, A.S.; Temu, E.B. (2012). Geodynamic significance of the TRM segment in the East African Rift (W-Tanzania): Active tectonics and paleostress in the Ufipa plateau and Rukwa basin. *Journal of Structural Geology*, *37*, 161-180. https://doi.org/10.1016/j.jsg.2012.01.008 [Link]Unknown Author (2023). East African Community (EAC). *International Trade Statistics Yearbook (Ser. G)*, 22-22. https://doi.org/10.18356/9789210027878c024 [Link]Unknown Author (1998). Vingt après (en russe). *Villes en parallèle*, *26*(1), 235-250. https://doi.org/10.3406/vilpa.1998.1264 [Link]Cardone, D.; Perrone, G. (2015). Damage and Loss Assessment of Pre-70 RC Frame Buildings with FEMA P-58: A Case Study. *Improving the Seismic Performance of Existing Buildings and Other Structures 2015*, 363-375. https://doi.org/10.1061/9780784479728.030 [Link]Goda, Katsuichiro (2020). Multi-Hazard Portfolio Loss Estimation for Time-Dependent Shaking and Tsunami Hazards. *Frontiers in Earth Science*, *8*. https://doi.org/10.3389/feart.2020.592444 [Link]Makoni, Munyaradzi (2022). New Hazard Exposure Model for Africa. *Eos*, *103*. https://doi.org/10.1029/2022eo220170 [Link]Arya, Anand Swarup (2018). Earthquake Resistant Design of Masonry Buildings. *Advances in Indian Earthquake Engineering and Seismology*, 259-271. https://doi.org/10.1007/978-3-319-76855-7_12 [Link]Lindenfeld, Michael; Rümpker, Georg (2011). Detection of mantle earthquakes beneath the East African Rift. *Geophysical Journal International*, *186*(1), 1-5. https://doi.org/10.1111/j.1365-246x.2011.05048.x [Link]Pagani, M.; Monelli, D.; Weatherill, G.; Danciu, L.; Crowley, H.; Silva, V.; Henshaw, P.; Butler, L.; Nastasi, M.; Panzeri, L.; Simionato, M.; Vigano, D. (2014). OpenQuake Engine: An Open Hazard (and Risk) Software for the Global Earthquake Model. *Seismological Research Letters*, *85*(3), 692-702. https://doi.org/10.1785/0220130087 [Link]Poggi, Valerio; Durrheim, Raymond; Tuluka, Georges Mavonga; Weatherill, Graeme; Gee, Robin; Pagani, Marco; Nyblade, Andrew; Delvaux, Damien (2017). Assessing seismic hazard of the East African Rift: a pilot study from GEM and AfricaArray. *Bulletin of Earthquake Engineering*, *15*(11), 4499-4529. https://doi.org/10.1007/s10518-017-0152-4 [Link]Suarez, Vinicio; Kowalsky, Mervyn J. (2007). Displacement-Based Seismic Design of Drilled Shaft Bents with Soil-Structure Interaction. *Journal of Earthquake Engineering*, *11*(6),

1010-1030. https://doi.org/10.1080/13632460701232683 [Link]Seyhan, Emel; Stewart, Jonathan P. (2014). Semi-Empirical Nonlinear Site Amplification from NGA-West2 Data and Simulations. *Earthquake Spectra*, *30*(3), 1241-1256. https://doi.org/10.1193/063013eqs181m [Link]Booth, Edmund (2014). Seismic isolation. *Earthquake Design Practice for Buildings*, 295-314. https://doi.org/10.1680/edpb.57944.295 [Link]Jara, J.M.; Álvarez, O.; Jara, M.; Olmos, B.A. (2016). Seismic vulnerability of retrofitted bridges. *Maintenance, Monitoring, Safety, Risk and Resilience of Bridges and Bridge Networks*, 462-462. https://doi.org/10.1201/9781315207681-279 [Link]Kean, Jason; Kostelnik, Jaime; Jones, Eric S.; Rengers, Francis; Hoch, Olivia (2022). THE USGS LANDSLIDE HAZARDS PROGRAM'S RESPONSE TO THE 2022 WILDFIRES IN NEW MEXICO. *Geological Society of America Abstracts with Programs*. https://doi.org/10.1130/abs/2022am-378673 [Link]Unknown Author (2015). Federal Emergency Management Agency (FEMA). *Encyclopedia of Trauma Care*, 607-607. https://doi.org/10.1007/978-3-642-29613-0_100622 [Link]